WILEY-VCH

DOI: 10.1002/smll.201600311
Article type: Full Paper

Co-Immobilization of Proteins and DNA Origami Nanoplates to Produce High-Contrast Biomolecular Nanoarrays

Robert Hager,[1] Jonathan R. Burns,[2] M. Grydlik,[3] A. Halilovic,[3] T. Haselgrübler,[1] Friedrich Schäffler,[3] Stefan Howorka[1,2]*

[1] Center for Advanced Bioanalysis GmbH, 4020 Linz, Austria, [2] Department of Chemistry, Institute of Structural and Molecular Biology, University College London, London, England, United Kingdom, [3] Institute for Semiconductor and Solid State Physics, Johannes Kepler University, 4040 Linz, Austria

corresponding author: s.howorka@ucl.ac.uk, 0044 20 7679 4702

Keywords: nanopattern, biofunctionalization, DNA origami, protein, fluorescence microscopy

The biofunctionalization of nanopatterned surfaces with structurally defined DNA origami is an important topic in nanobiotechnology. An unexplored challenge is, however, to co-immobilize proteins with DNA origami of usually different charge characteristics at pre-determined substrate sites in high-contrast relative to the non-target areas, and preferably on a transparent substrate to allow ultrasensitive optical detection. If successful, specific co-immobilization would be a step towards stoichimetricaly defined arrays with few to individual protein molecules per site. Here we achieve an important requirement towards this aim by successfully co-immobilizing with high specificity positively charged avidin proteins and negatively charged DNA origami nanoplates on 100 nm-wide carbon nanoislands while suppressing undesired adsorption to surrounding non-target areas. The arrays on glass slides achieve unprecedented selectivity factors of up to 4000 and allow ultrasensitive fluorescence read-out. The co-immobilization onto the nanoislands leads to layered biomolecular architectures which are functional because bound DNA origami influences the number of capturing sites on the nanopatches for other proteins. The novel hybrid DNA origami-protein nanoarrays allow the fabrication of versatile research platforms for applications in biosensing, biophysics and cell biology, and, in addition, represent an important stepping stone to single-molecule proteins arrays.

1. Introduction

Patterned surfaces displaying protein or DNA molecules on defined nanoscale sites play a major role in modern sequencing and diagnostic sensing applications as well as in biophysical and cell biological research.[1-7] The nanoarrays are usually obtained by first fabricating chemically adhesive nanopatches via serial writing or parallel fabrication methods and then by adsorbing biomolecules onto these sites.[8-10]

A powerful strategy to enhance nanoarrays is to co-immobilize protein and DNA in order to exploit the unique properties of the two biopolymers. Of particular interest is the deposition of highly structured bottom-up DNA origami nanomaterials that complement the atomically ill-defined top-down nanopatches.[11-15] The rationally designed DNA nanostructures offer excellent control over molecular dimensions[16-21] and can bind in defined stoichiometry or molecular orientation on the nanoislands.[11-13, 22] DNA origami have also been used as nanoscale immobilization platforms for smaller molecular cargo including proteins,[23-26] [27-30] but in this case the platforms were only randomly bound to the substrate surface.

While not yet realized, co-immobilization of DNA origami and proteins on nanopatterned surfaces can advance nanobiotechnology. The expected scientific benefits stem from synergistically combining the nanoscale precision of DNA origami with the proteins' wide functional breadth, superior molecular recognition, and efficient enzymatic catalysis.[14] For example, co-binding could help form useful hierarchical multi-component assemblies which can be applied to tune the number of proteins per nanopatch.[31] This is of relevance in biosensing and research. Co-immobilization will ultimately also enable the production of single-protein arrays where an individual protein is positioned on one nanoisland.[31]

Achieving these ambitious aims requires, however, to tackle the fundamental step of selectively binding DNA as well as protein onto the inorganic nanopatches. This is experimentally demanding as the two classes of biomolecules have radically different chemical compositions, shapes, and molecular surface characteristics such as charge distribution. Consequently, problems can result because nanopatches of conventional monofunctional coupling chemistries usually capture well only one class of biomolecule.[32-34] Another and often more severe issue is that non-target areas surrounding the nanosites as well as the incubation protocols are tailored to prevent non-specific binding of either DNA or proteins but not both.[35] As a consequence, exposure to protein and DNA can result in low-contrast biomolecular nanopatterns and insufficient signal-to-noise ratios in read-out. This is of particular relevance when ultra-sensitive read-out via fluorescence microscopy is required.

Here we create advanced nanoarrays that spatially co-immobilize DNA origami nanoplates and proteins in unprecedented high contrast relative to the surrounding non-target areas. Key for achieving low non-specific binding to non-target areas is the use of a polymeric nanofilm of dual-passivating properties, as well as optimized incubation conditions. By comparison, protein and DNA plates bound on target nanoislands form a hierarchically structured nanoassembly. The functional performance of the assemblies is also demonstrated by showing that DNA plates tune and reduce the number of additional proteins per nanopatch. Our study lays the foundation for future work aimed at controlling the number of protein molecules down to individual copies as well as their position on the nanoisland which is of considerable interest in biosensing, biophysics and cell biology.

2. Results

2.1. Principle of Forming DNA-Origami and Protein-Decorated Nanoarrays

The formation of the protein- and DNA origami-functionalized nanoarrays is schematically illustrated for a single square nanoisland in **Figure 1**. In step 1, islands composed of carbon (Figure 1, dark grey) are written with an electron-beam. The substrate for e-beam writing is covered with a dense and charge-neutral poly(ethylene glycol) (PEG) film (Figure 1, green area) to prevent non-specific adsorption of biomolecules. By contrast, the negatively polarized carbon islands are adhesive for proteins whereby those with a higher net positive charge (i.e. high isoelectric point, pI) bind at greater local density than neutral or net negatively charged polypeptides. A previous study has used e-beam writing to create nanoarrays for protein binding,[31] but the fabrication of nanoislands decorated with protein and DNA origami using a dual-passivating PEG film has not been demonstrated before.

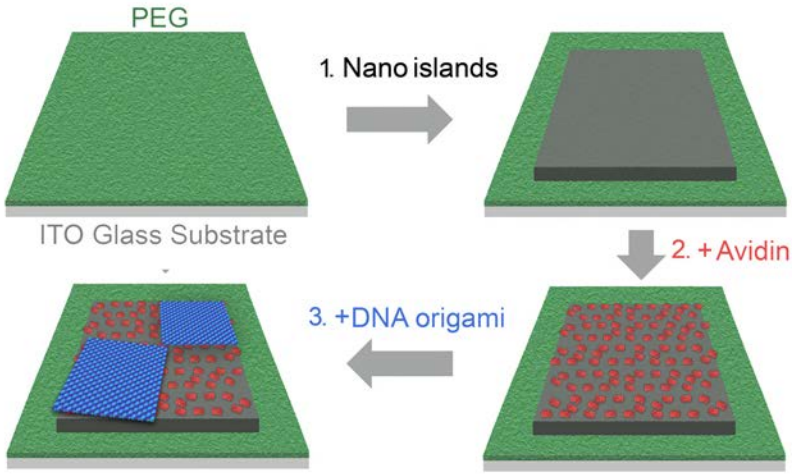

Figure 1. Scheme illustrating the fabrication of carbon nanoislands via e-beam induced deposition (EBID), and the biofunctionalization of negatively polarized islands via electrostatic layer-by-layer coating with positively charged avidin protein followed by negatively charged DNA origami nanoplates. The ITO-glass substrate is coated with a PEG

film to prevent non-specific binding of protein and DNA origami. For reasons of visual clarity, only a single island is shown. The procedure involves (1) EBID-writing of carbon nanoislands, (2) coating of islands with protein avidin, (3) electrostatic binding of DNA origami nanoplates to the avidin layer. Note that the DNA plates are depicted in planar form for simplicity but we do not rule out that they become corrugated as found at high cation densities.[36]

Consequently, follow-on incubation of the nanopatterned substrate with net positively charged avidin (pI = 10.5)(Figure 1, step 2, red) causes the protein to adsorb onto the islands but not to the surrounding areas. In a similar fashion, negatively charged DNA origami plates (pI = 1.5) of 50 x 50 nm lateral size (Figure 1, step 3, blue squares) bind electrostatically to the avidin-coated islands to give rise to the hierarchical two-layer assembly. In this configuration, avidin serves as an electrostatic adhesive to bind DNA plates to the nanoislands. Non-specific adsorption of the DNA plates to the surrounding PEG film is suppressed. The DNA origamis can, in a future development, be modified to display few to individual copies of other protein molecules.

2.2. Electron-Beam-Deposition Writing of Carbon Nanoislands

As substrates for the top-down nanofabrication step (Figure 1, step 1), we used indium tin oxide (ITO)-coated glass slides that were covered with a PEG film. ITO is a suitable substrate for e-beam writing because it dissipates electrical current, and is additionally optically transparent to allow ultransensitive fluorescence read-out of adsorbed biomolecules.[37] The PEG film was formed by silanization of the substrate,[35, 37] and was subjected to surface analytical characterization to confirm its chemical identity, expected thickness, lateral homogeneity, porosity, and passivation properties.[38]

The carbon nanoislands with nominal dimensions of 100 x 100 nm were written via e-beam-induced deposition (EBID) of carbon (Figure 1, step 1).[39, 40] In this patterning approach, the focused e-beam causes the localized decomposition of the PEG-film and the simultaneous deposition of the reduced carbon at the irradiated substrate sites.[40] The effect is mediated by primary electrons in the topmost few nanometer of the substrate, and by backscattered electrons from the excitation volume.[39, 40] As main advantage, EBID gives excellent control over the lateral position of the nanoislands, as well as their lateral size and height. Above a threshold, the height increases with higher electron doses. As this also leads to a larger amount of bound protein,[41, 42] e-dose is hence an ideal experimental parameter to tune the surface-density of protein on the islands.[31] Here we use e-beam dose as a tool to identify which does are ideal to achieve a high specificity in the formation of DNA nanoarrays.

To confirm that the EBID nanostructures had been successfully written, analysis via atomic force microscopy (AFM) was applied. For AFM, the islands were written on atomically flat silicon because the ITO surface with an rms roughness of 1 nm[37] does not permit visualization of the nanofeatures. **Figure 2** shows an AFM image for an array of nanoislands written at an electron acceleration voltage of 20 kV and an electron dose of 1.16 pC. The lateral size of the square islands (Figure 2, inset) was 98.3 ± 11.7 nm (n = 9) in agreement with the nominal dimensions of 100 x 100 nm, and the height of the islands was 3.3 ± 0.5 nm above the ITO surface. The dependence of nanoisland height on electron dose has been published previously.[31] The pitch between the islands was set at 3.2 µm, i.e. above the diffraction limit to optically resolve the islands with fluorescence microscopy.

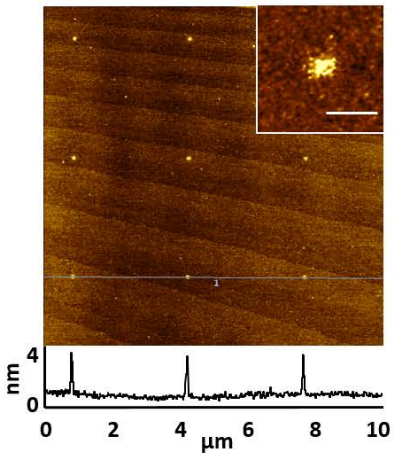

Figure 2. Atomic force microscopy image and height profile of 100 nm x 100 nm EBID nanoislands written on a silicon substrate. The nanofeatures were generated using an electron dose of 1.16 pC. Inset: 500 x 500 nm, scale bar: 200 nm.

2.3. Biofunctionalizing Carbon Nanoislands with Avidin Protein

To demonstrate the selective adsorption of protein to the nanoislands (Figure 1, step 2; **Figure 3A**), nanoarrays composed of 10 x 10 islands were incubated with avidin labeled with fluorophore Cy3. We used a series of arrays written on ITO-substrates with e-beam doses covering a 100-fold range. Fluorescence microscopic analysis confirmed that higher doses led to more protein binding (Figure 3B). All islands of a representative array of a given dose were biofunctionalized with avidin protein (Figure 3C, 2.9 pC; SI, all doses in Figure S2). Within each array, the fluorescence distribution was narrow (Figure 3D) implying that roughly equal amounts of protein had bound to the islands. Avidin-Cy3 adsorbed with high affinity, *A*, to the carbon islands, whereby *A* relates to the amount of biomolecules bound per island (Figure 3E). *A* is calculated from the difference of the average fluorescence of a 10 x 10 array of 100 x 100 nm^2 islands covering a total area of 39 x 39 μm^2, and the average background fluorescence from an proximal area without islands. Affinity thus represents the fluorescence of the island minus background flurorescence.The affinity increased with e-dose and reached a value of

290 at 2.9 pC. Similarly, the binding proceeded with high specificity, *S*, which describes how many biomolecules bind per island in relation to the surrounding PEG surface of the same area (Figure 3). Sensitivity *S* is calculated from the ratio of the net fluorescence (affinity) over the background fluorescence, including a normalization factor to accout for the different areas of nanoislands (100 x 10^4 nm^2) vs. surrounding PEG-coated area of 39 x 39 μm^2. Indeed, at maximum doses *S* reached unprecedented high values of up to 4000 (Figure 3F). A high value was also obtained when using the alternative contrast factor (SI, Figure S3)[43]. Neither *A*, *S*, nor the contrast factor are equivalent to the number of adsorbed avidin molecules. This value was not experimentally determined but the theoretically maximum loading capacity is 500 avidin molecules per island assuming tightly packed proteins. The high affinity to target islands and the low amount of non-specifically bound protein are the result of an optimization of the buffer condition used for the incubation step. The results for other buffer conditions are described in the SI, Figure S4. We note that our analysis via affinity and selectivity relies on the assumption that carbon nanoislands and PEG-coated ITO areas have no differential influence on fluorescence emission. The equality has been experimentally demonstrated previously[31] even though a more recent study found that ITO can have a distance-dependence quenching effect on fluorophores.[44] The impact will, however, be limited for this data set as both carbon islands and water-hydrated PEG-layer[45] have the same distance to and height above the ITO substrate with a value of 3-4 nm.

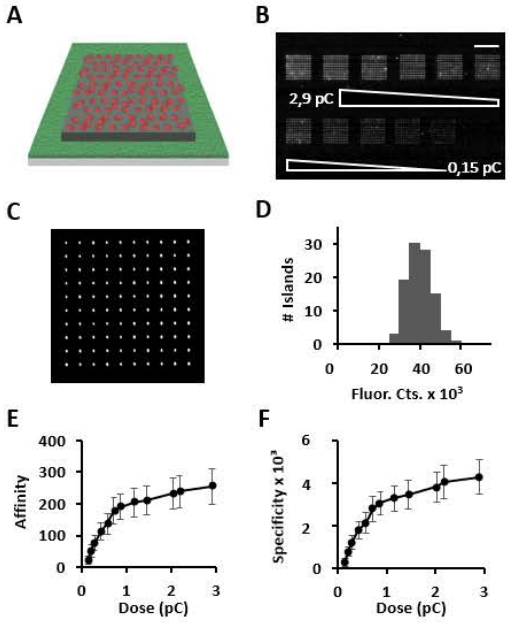

Figure 3. Avidin binding to carbon nanoislands is homogenous and increases with the EBID electron dose. (A) Schematic representation of a single island decorated with avidin-Cy3. (B) Fluorescence microscopic image of arrays of 10 x 10 islands of 100 x 100 nm dimensions which were decorated with avidin-Cy3. Islands within an array were written with the same electron dose while the dose was varied between arrays between 2.9 pC to 0.15 pC. Scale bar: 32 µm. (C) Image of one array written at 2.9 pC. Image size: 39 x 39 µm. (D) Histogram of the fluorescence distribution of the islands in (C). (E) Affinity *A* and (F) specificity *S* depend on the electron dose used for writing of EBID-carbon nanoislands. The data in E and F represent the averages and standard deviations of 8 independent experiments.

2.4. Decorating Avidin-Coated Nanoislands with DNA-Origami Nanoplates

For the next incubation step (Figure 1, step 3) we designed a DNA origami nanoplate composed of a single-duplex layer with nominal dimensions of 2 x 50 x 50 nm **(Figure 4A)**. The DNA nanoplate was assembled via the scaffold-and-staple strategy[17] which involves

annealing of the long scaffold with excess short staple strands by heating and cooling. The annealing was successful as shown by agarose gel electrophoresis (Figure 4B; SI, Figure S5) because the product migrated as a defined single gel band in a position different to the scaffold strand (Figure 4B, lanes 3 and 2, respectively; product defined with red arrow). Excess staple strands that migrated faster in the gel (Figure 4B, lane 3) were successfully removed by filtration (Figure 4B, lane 1). AFM analysis established the expected square dimensions of the DNA nanoplate (Figure 4C; length, 51.7 ± 2.4 nm; width 45.8 ± 3.6 nm; height 1.1 ± 0.2; n =11). To facilitate subsequent detection with fluorescence microscopy, four Alexa 532-modified oligonucleotides were attached to the corners of the plate via DNA hybridization (Figure 4A).

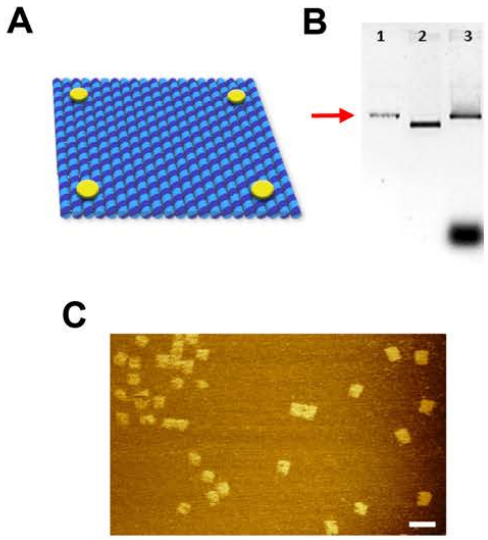

Figure 4. Formation and characterization of DNA origami nanoplates. (A) Schematic drawing of a DNA nanoplate of 50 x 50 nm carrying a fluorophore in each corner. (B) Gel electropherogram of DNA nanoplates: lane 1, purified DNA origami; lane 2, M13mp18 scaffold strand; lane 3, DNA origami plates before purification to remove staple strands. (C) AFM image of DNA nanoplates adsorbed on mica. Scale bar: 100 nm.

The binding of fluorophore-tagged DNA nanoplates to avidin-coated islands (Figure 1, step 3; **Figure 5A**) was examined using fluorescence microscopy. The corresponding image of a single array (Figure 5B, written at 2.9 pC) shows that 97 % of the islands were covered. The corresponding fluorescence histogram for the decorated islands (Figure 5C) implies a narrow distribution skewed towards lower fluorescence. Electrostatic interaction was the main reason for binding of DNA nanoplates because negatively charged single stranded DNA oligonucleotides also co-localized to the avidin-coated islands but not to islands without the protein layer (SI, Figure S6). The binding of DNA origami is also supported by analysis of the AFM height profiles (SI, Figure S7). The net height increase caused by DNA origami was 3.8 ± 3.6 nm which is higher than the theoretical height of 2 nm of the plates. While within experimental error, the discrepancy may imply that DNA origami nanoplates deviate from the expected flat appearance and are locally crumpled. This was found for plates exposed to a higher cation density[36] but a direct comparison is not possible as the study adsorbed plates to graphene and not a protein layer as in our report.

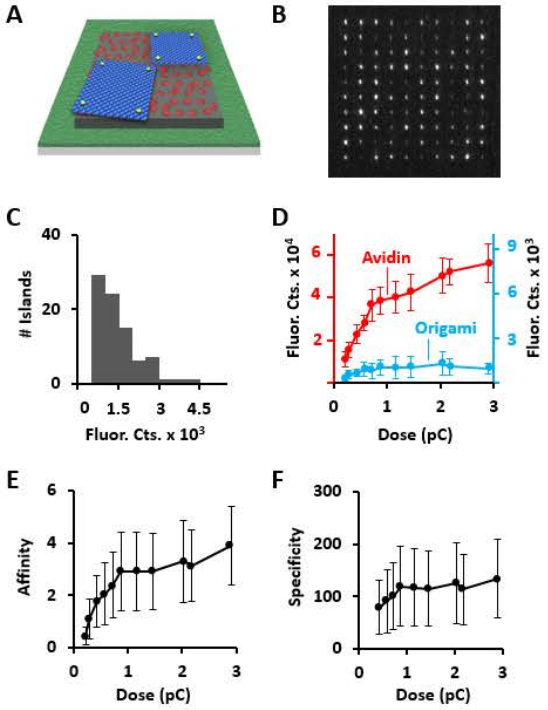

Figure 5. Binding of fluorescence-labeled DNA origami to carbon nanoislands coated with non-fluorescent avidin. (A) Schematic drawing of DNA nanoplates bound to an avidin-coated EBID structure. The DNA nanoplates may deviate from the flat rectangular shape and be more corrugated. (B) Fluorescence image of an array of 10 x 10 islands of 100 x 100 nm written at a dose of 2.9 pC (image size: 39 x 39 μm). (C) Fluorescence intensity distribution of islands in (B). (D) Plot of mean fluorescence intensity vs electron dose for DNA origami (blue) and avidin-Cy3 (red). Affinity (E) and specificity (F) of DNA origami vs electron dose.

Further examination using fluorescence microscopy showed that the surface coverage of islands with DNA plates directly correlates with the electron dose (SI, Figure S8). However, above a threshold value of 0.5 pC, the dose did not drastically alter the extent of DNA nanoplates binding per island (Figure 5D, blue). This saturation suggests that the maximum number of 50 x 50 nm plates per 100 x 100 nm island cannot increase beyond 3-4 due to steric exclusion. By contrast, the amount of smaller avidin (4 x 5 x 6 nm) scaled much stronger with dose (Figure 5D, red) implying that saturation had not been reached due to the

much higher theoretically loading capacity of 500 avidin molecules per island. As additional analysis, the plot of affinity *A* for DNA origami as a function of electron dose (Figure 5E) featured lower values compared to avidin (Figure 4E), reflecting the lower number of bound DNA origami than proteins. Similarly, specificity *S* was weakly influenced by dose and reached a maximum of 120 (Figure 5F). This is lower than for avidin but still good when compared to other studies of DNA origami binding to physical nanopatterns.[12, 13] The larger error bars in plots of Figures 5E & F do not reflect inconsistent results but are due to the expected variation when very few DNA origami molecules bind per island. In agreement, a smaller error was obtained in the affinity and selectivity plots for the binding of DNA oligonucleotides because a much larger number of strands bind per island (SI, Figure S6). In a next future step, these island-bound DNA nanoplates may be used as a molecular platform to display defined number of protein molecules. But this extended approach is outside the scope of this study.

2.5. Demonstrating the Functionality of the Hierarchical Protein-DNA Assemblies

We sought to demonstrate the functionality of the hierarchical protein-DNA assemblies using an approach which is different to the direct use of DNA plates as display platforms. Rather, we used DNA origamis as mask to tune binding of another model protein. It was expected that islands with bound DNA plates would have a lower binding capacity for additional protein (**Figure 6A**, yellow protein) compared to islands that had only been exposed to avidin (Figure 6B). As a probe protein, fluorescence-labeled streptavidin was used and incubated on nanoisland arrays. Streptavidin has a pI of 5 and is not anticipated to bind to the negatively charged DNA but only to the non-covered areas of the nanoisland. To enable specific detection of bound streptavidin, the arrays had been decorated with non-fluorescent avidin and, optionally, non-labeled DNA origami.

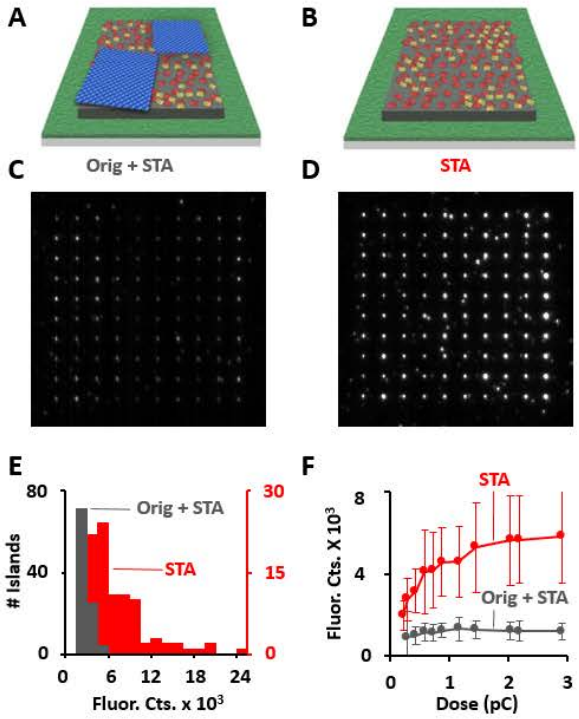

Figure 6. The binding capacity of nanoislands for streptavidin (STA, yellow) is reduced by the presence of DNA origami plates. Streptavidin bound onto (A) islands coated with avidin (red) and DNA origami (blue) and (B) islands coated with avidin. (C, D) Fluorescence images of island arrays with (C) and without (C) DNA origami plates. (E) Fluorescence intensity distribution of micrographs of islands decorated with streptavidin and DNA origami (grey, corresponding micrograph C) and islands with streptavidin (red, corresponding micrograph D). (F) Plot of mean fluorescence intensity against electron dose for DNA origami + streptavidin (grey), and streptavidin (red).

Fluorescence scanning established that islands with DNA plates (Figure 6C) had a much lower fluorescence intensity than islands without plates (Figure 6D), in line with expectations. The difference was also apparent in fluorescence histogram analysis (Figure 6E). The striking influence of DNA origami was also apparent when comparing the mean fluorescence of

decorated islands as a function of electron dose (Figure 6F). In line with expectations for a limited number of binding sites, fluorescence at DNA plate-covered islands leveled off at a much lower dose than for islands without plates. Some streptavidin protein also bound outside the target areas (Figure 6D). Likely, this increase in non-specific binding is due to repeated challenging of the substrate surfaces with other proteins and DNA. But non-specific binding may be compensated by including mild detergents in the incubation buffer.

3. Conclusions

In this report, we have generated nanoarrays of hierarchically controlled assemblies of DNA origami nanoplates and proteins bound on nanoislands. Our study addresses the demand for higher-order nanoarrays that synergistically combine top-down physical nanopatterns and bottom-up DNA origami nanostructures. The highlights of the report are: (i) With the use of dual-passivating PEG nanofilms, the study achieved very high specific binding of biomolecules onto nanoislands with unprecedented high selectivity factor of up to 4000. Given the reduction of non-specific binding to non-target areas, the report (ii) pioneered the decoration of nanoislands with DNA origami and proteins. Previously, only protein or DNA origami but not both were bound to the islands. Our study (iii), paves the way to exploit DNA nanoplates to produce arrays of few to single molecules. In this route, DNA plates with a size matching the nanoislands will be used to display a defined number of molecules.[10] The principle of molecular display has been previously demonstrated with proteins carrying the widely used hexahistidine tag and their coupling to the metal chelate NTA tags that are chemically attached to DNA nanoplates.[19, 26] However, protein-decorated DNA plates were not yet bound specifically to top-down fabricated nanopatterns. We anticipate this can be achieved with our nanoarrays and the dual-passivating PEG films. The advantage is that the

route is compatible with a wide range of proteins, because the PEG surfaces and nanoislands can cope with extreme cases of proteins in terms of charge as shown in our report. Hence, proteins with intermediate isoelectric points can be used including antibodies, enzymes or even cell-stimulating peptides.[31] Once produced, these nanoarrays could boost cell biological investigations by presenting to cells few to individual activating proteins at spots at defined micro- to nanoscale spacing. Based on our present work, the most promising route towards single-molecule arrays will be to decorate top-down patterns of 50 nm feature size with atomically precise DNA origamis of matching dimensions. Finally, our study (iv) introduces a new approach to use DNA origami independent to the classical "direct" role as molecular display platforms.[11, 25] The alternative strategy termed "indirect" uses DNA platforms as masks to cover part of the nanoislands and thereby lead to the reduced binding of proteins on sites not blocked by the DNA plates. We expect that the "indirect" strategy can prove useful when the nanoislands are generated with patterning methods that either cannot produce nanofeatures smaller than 100 nm or are unable to tune the binding density for protein, unlike EBID in our study. One prime candidate of a simple method that can benefit of the "indirect" use of DNA plates is highly parallel nanostamping.[46] In conclusion, our report advances the field of nanobiotechnology and nanostructured surface and provides an important step towards valuable tools for cell biological and biophysical research.

Supporting Information

Supporting Information including experimental methods and experimental results is available from the Wiley Online Library or from the author.

Acknowledgements

We acknowledge support by the Austrian Science Foundation (P 25730-B21). S.H. also acknowledges support by the Province of Upper Austria, and the European Regional Development Fund (EFRE).

References

[1] R. Drmanac, A. B. Sparks, M. J. Callow, A. L. Halpern, N. L. Burns, B. G. Kermani, P. Carnevali, I. Nazarenko, G. B. Nilsen, G. Yeung, F. Dahl, A. Fernandez, B. Staker, K. P. Pant, J. Baccash, A. P. Borcherding, A. Brownley, R. Cedeno, L. Chen, D. Chernikoff, A. Cheung, R. Chirita, B. Curson, J. C. Ebert, C. R. Hacker, R. Hartlage, B. Hauser, S. Huang, Y. Jiang, V. Karpinchyk, M. Koenig, C. Kong, T. Landers, C. Le, J. Liu, C. E. McBride, M. Morenzoni, R. E. Morey, K. Mutch, H. Perazich, K. Perry, B. A. Peters, J. Peterson, C. L. Pethiyagoda, K. Pothuraju, C. Richter, A. M. Rosenbaum, S. Roy, J. Shafto, U. Sharanhovich, K. W. Shannon, C. G. Sheppy, M. Sun, J. V. Thakuria, A. Tran, D. Vu, A. W. Zaranek, X. Wu, S. Drmanac, A. R. Oliphant, W. C. Banyai, B. Martin, D. G. Ballinger, G. M. Church, C. A. Reid, *Science* **2010**, *327*, 78.

[2] P. M. Mendes, C. L. Yeung, J. A. Preece, *Nanoscale Res. Lett.* **2007**, *2*, 373.

[3] D. W. Schmidtke, Z. R. Taylor, K. Patel, T. G. Spain, J. C. Keay, J. D. Jernigen, E. S. Sanchez, B. P. Grady, M. B. Johnson, *Langmuir* **2009**, *25*, 10932.

[4] K. L. Christman, V. D. Enriquez-Rios, H. D. Maynard, *Soft Matt.* **2006**, *2*, 928.

[5] J. D. Ding, J. H. Huang, S. V. Grater, F. Corbellinl, S. Rinck, E. Bock, R. Kemkemer, H. Kessler, J. P. Spatz, *Nano Lett.* **2009**, *9*, 1111.

[6] H. Agheli, J. Malmstrom, E. M. Larrson, M. Textor, D. S. Sutherland, *Nano Lett.* **2006**, *6*, 1165.

[7] M. P. Lutolf, P. M. Gilbert, H. M. Blau, *Nature* **2009**, *462*, 433.

[8] C. A. Mirkin, C. M. Niemeyer, *Nanobiotechnology II: More concepts and applications*, John Wiley & Sons, **2007**.

[9] C. M. Niemeyer, C. A. Mirkin, *Nanobiotechnology: Concepts, applications and perspectives*, John Wiley & Sons, **2004**.

[10] S. Howorka, J. Hesse, *Soft Matt.* **2014**, *10*, 931.

[11] M. B. Scheible, G. Pardatscher, A. Kuzyk, F. C. Simmel, *Nano Lett.* **2014**, *14*, 1627.

[12] R. J. Kershner, L. D. Bozano, C. M. Micheel, A. M. Hung, A. R. Fornof, J. N. Cha, C. T. Rettner, M. Bersani, J. Frommer, P. W. K. Rothemund, G. M. Wallraff, *Nat. Nanotechnol.* **2009**, *4*, 557.

[13] A. M. Hung, C. M. Micheel, L. D. Bozano, L. W. Osterbur, G. M. Wallraff, J. N. Cha, *Nat. Nanotechnol.* **2010**, *5*, 121

[14] S. Howorka, *Langmuir* **2013**, *29*, 7344.

[15] B. Teshome, S. Facsko, A. Keller, *Nanoscale* **2014**, *6*, 1790.

[16] J. Zheng, J. J. Birktoft, Y. Chen, T. Wang, R. Sha, P. E. Constantinou, S. L. Ginell, C. Mao, N. C. Seeman, *Nature* **2009**, *461*, 74.

[17] P. W. Rothemund, *Nature* **2006**, *440*, 297.

[18] A. J. Wollman, C. Sanchez-Cano, H. M. Carstairs, R. A. Cross, A. J. Turberfield, *Nat. Nanotechnol.* **2014**, *9*, 44.

[19] B. Sacca, C. M. Niemeyer, *Chem. Soc. Rev.* **2011**, *40*, 5910.

[20] E. S. Andersen, M. Dong, M. M. Nielsen, K. Jahn, R. Subramani, W. Mamdouh, M. M. Golas, B. Sander, H. Stark, C. L. Oliveira, J. S. Pedersen, V. Birkedal, F. Besenbacher, K. V. Gothelf, J. Kjems, *Nature* **2009**, *459*, 73.

[21] T. Omabegho, R. Sha, N. C. Seeman, *Science* **2009**, *324*, 67.

[22] A. M. Hung, H. Noh, J. N. Cha, *Nanoscale* **2010**, *2*, 2530.

[23] B. Sacca, C. M. Niemeyer, *Angew. Chem. Int. Ed.* **2012**, *51*, 58.

[24] B. Sacca, R. Meyer, M. Erkelenz, K. Kiko, A. Arndt, H. Schroeder, K. S. Rabe, C. M. Niemeyer, *Angew. Chem. Int. Ed.* **2010**, *49*, 9378.

[25] S. Rinker, Y. G. Ke, Y. Liu, R. Chhabra, H. Yan, *Nat. Nanotechnol.* **2008**, *3*, 418.
[26] W. Q. Shen, H. Zhong, D. Neff, M. L. Norton, *J. Am. Chem. Soc.* **2009**, *131*, 6660.
[27] S. H. Park, P. Yin, Y. Liu, J. H. Reif, T. H. LaBean, H. Yan, *Nano Lett.* **2005**, *5*, 729.
[28] Y. He, Y. Tian, A. E. Ribbe, C. D. Mao, *J. Am. Chem. Soc.* **2006**, *128*, 12664.
[29] R. Chhabra, J. Sharma, Y. G. Ke, Y. Liu, S. Rinker, S. Lindsay, H. Yan, *J. Am. Chem. Soc.* **2007**, *129*, 10304.
[30] B. A. R. Williams, K. Lund, Y. Liu, H. Yan, J. C. Chaput, *Angew. Chem. Int. Ed.* **2007**, *46*, 3051.
[31] R. Schlapak, J. Danzberger, T. Haselgrubler, P. Hinterdorfer, F. Schaffler, S. Howorka, *Nano Lett.* **2012**, *12*, 1983.
[32] G. MacBeath, S. L. Schreiber, *Science* **2000**, *289*, 1760.
[33] J. P. Pellois, X. Zhou, O. Srivannavit, T. Zhou, E. Gulari, X. Gao, *Nat. Biotechnol.* **2002**, *20*, 922.
[34] S. Fukui, T. Feizi, C. Galustian, A. M. Lawson, W. Chai, *Nat. Biotechnol.* **2002**, *20*, 1011.
[35] R. Schlapak, D. Armitage, N. Saucedo-Zeni, W. Chrzanowski, M. Hohage, D. Caruana, S. Howorka, *Soft Matt.* **2009**, *5*, 613.
[36] J. M. Yun, K. N. Kim, J. Y. Kim, D. O. Shin, W. J. Lee, S. H. Lee, M. Lieberman, S. O. Kim, *Angew. Chem. Int. Ed.* **2012**, *51*, 912.
[37] R. Schlapak, D. Armitage, N. Saucedo-Zeni, M. Hohage, S. Howorka, *Langmuir* **2007**, *23*, 10244.
[38] R. Schlapak, D. Caruana, D. Armitage, S. Howorka, *Soft Matt.* **2009**, *5*, 4104.
[39] A. N. Broers, W. W. Molzen, J. J. Cuomo, N. D. Wittels, *Appl. Phys. Lett.* **1976**, *29*, 596.
[40] N. Silvis-Cividjian, C. W. Hagen, P. Kruit, M. A. J. v. d. Stam, H. B. Groen, *Appl. Phys. Lett.* **2003**, *82*, 3514.
[41] J. Rundqvist, J. H. Hoh, D. B. Haviland, *Langmuir* **2006**, *22*, 5100.
[42] B. Gao, G. H. Bernstein, M. Lieberman, *J. Vac. Sci. Technol. B* **2009**, *27*, 2292.
[43] M. Schwarzenbacher, M. Kaltenbrunner, M. Brameshuber, C. Hesch, W. Paster, J. Weghuber, B. Heise, A. Sonnleitner, H. Stockinger, G. J. Schütz, *Nature Methods* **2008**, *5*, 1053.
[44] R. J. Moerland, J. P. Hoogenboom, *optica* **2016**, *3*, 2334.
[45] C. L. Ren, R. Schlapak, R. Hager, I. Szleifer, S. Howorka, *Langmuir* **2015**, *31*, 11491.
[46] W. T. S. Huck, H. W. Li, B. V. O. Muir, G. Fichet, *Langmuir* **2003**, *19*, 1963.

Top-down carbon nanoarrays are biofunctionalized by highly specifically binding protein and bottom-up DNA-origami nanoplates. The hierarchical architectures can be used in biosensing, and biophysical and cell biological research.

Keywords: Nanoarray, DNA Origami

Robert Hager,[1] Jonathan R. Burns,[2] M. Grydlik,[3] A. Halilovic,[3] T. Haselgrübler,[1] Friedrich Schäffler,[3] Stefan Howorka[1,2*]

Co-Immobilization of Proteins and DNA Origami Nanoplates to Produce High-Contrast Biomolecular Nanoarrays

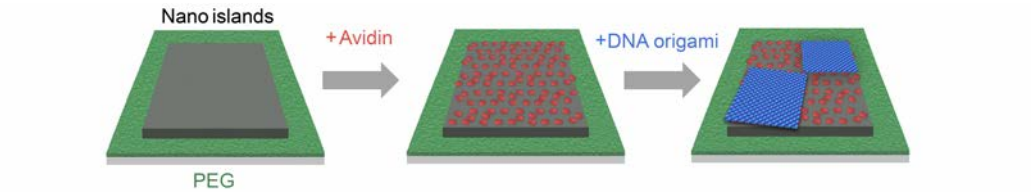

Copyright WILEY-VCH Verlag GmbH & Co. KGaA, 69469 Weinheim, Germany, 2013.

Supporting Information

Co-Immobilization of Proteins and DNA Origami Nanoplates to Produce High-Contrast Biomolecular Nanoarrays

Robert Hager,[1] Jonathan R. Burns,[2] M. Grydlik,[3] A. Halilovic,[3] T. Haselgrübler,[1] Friedrich Schäffler,[3] Stefan Howorka[1,2]*

[1] Center for Advanced Bioanalysis GmbH, 4020 Linz, Austria, [2] Department of Chemistry, Institute of Structural and Molecular Biology, University College London, London, England, United Kingdom, [3] Institute for Semiconductor and Solid State Physics, Johannes Kepler University, 4040 Linz, Austria,

* s.howorka@ucl.ac.uk, 0044 20 7679 4702

1. Materials and Methods

1.1. Reagents

Indium tin oxide (ITO)-coated glass slides (50 x 24 x 0.175 mm) with an ITO thickness of 17 ± 2 nm and a sheet resistance of 1200 ± 200 Ω/sq were obtained from Hans Tafelmaier Dünnschicht-Technik GmbH (Rosenheim, Germany). MeO-PEG-$(CH2)_3$-Si(O Me)$_3$ with a MW of 460-590 D was bought from ABCR (#SIM6492.7, Karlsruhe, Germany). Avidin-Cy3 conjugate (A4500-20) was purchased from USBiological (Swampscott, MA). Atto 550-Streptavidin (96404), Atto 655-Streptavidin (02744), Avidin (A9275) and Amicon Ultra centrifugal filter units (Z648043-24EA) were obtained from Sigma-Aldrich. GelRed™ Nucleic Acid Gel Stain (41003) was supplied by VWR International, and Agarose NEEO ultra-quality (2267.2) was purchased by Carl Roth. All DNA oligonucleotides were procured from IDT DNA technologies. Unmodified DNA oligonucleotide staples were supplied without additional purification on a 100 nmole scale and used at a concentration of 100 µM in deionized water. Dye-modified strands were synthesized on a 1 µmole scale with HPLC purification and dissolved in water to a final concentration of 100 µM. The scaffold strand m13mp18 was purchased from NEB.

1.2. Preparation of DNA Origami Plates

The 2D DNA map of the DNA nanoplate is shown in Figure S1. It contains the scaffold strand (blue), staple strands (red), and staple adapter strands (black) that carry 3'-terminal single-stranded extensions used to hybridize Alexa532-modified DNA oligonucleotide to the four corners of the DNA nanopore. The sequences of staple and adapter staple strands is provided in Table S1 and S2, respectively. The sequence of the dye-modified DNA oligonucleotide is 5'-CTCGCTTCTGTCTATCTTGGC-3' carrying an Alexa532 fluorophore via an amide bond linkage at the 5' terminus.

To prepare DNA origami plates, M13mp18 scaffold strand (40 µL, stock 100 nM, final concentration 8 nM), a mixture of staple strand (50 µL, stock 1 µM, final concentration 50 nM), and optionally Alexa532-modified DNA oligonucleotide and four adapter staple strands (12 µL and 2 µL corresponding to a final concentration of 1.2 µM and 200 nM, respectively) were added to 10 x PBS, 140 mM $MgCl_2$, pH 7.4 (100 µL) and deionized water (786 µL). The nanostructure was folded by heating the DNA solution to 85°C for 5 min and then cooling it to 5°C at a rate of 1°C/15 min using a PCR thermocycler with the lid temperature set to 90°C. For purification, excess staple strands were removed by molecular weight cut-off filtration with 100 kD spin filters. Therefore, 150 µL sample was mixed with 1850 µL TAE buffer supplemented with 14 mM $MgCl_2$, and centrifuged at 4000 g at 4 °C for 30 min. For additional purification cycles, the spin filter was filled again with 1850 µL buffer and centrifuged at the same conditions. Sample recovery was achieved by spinning the inverted filter unit for 5 min at 1000 g. The sample volume was then adjusted to the initial volume of sample before purification.

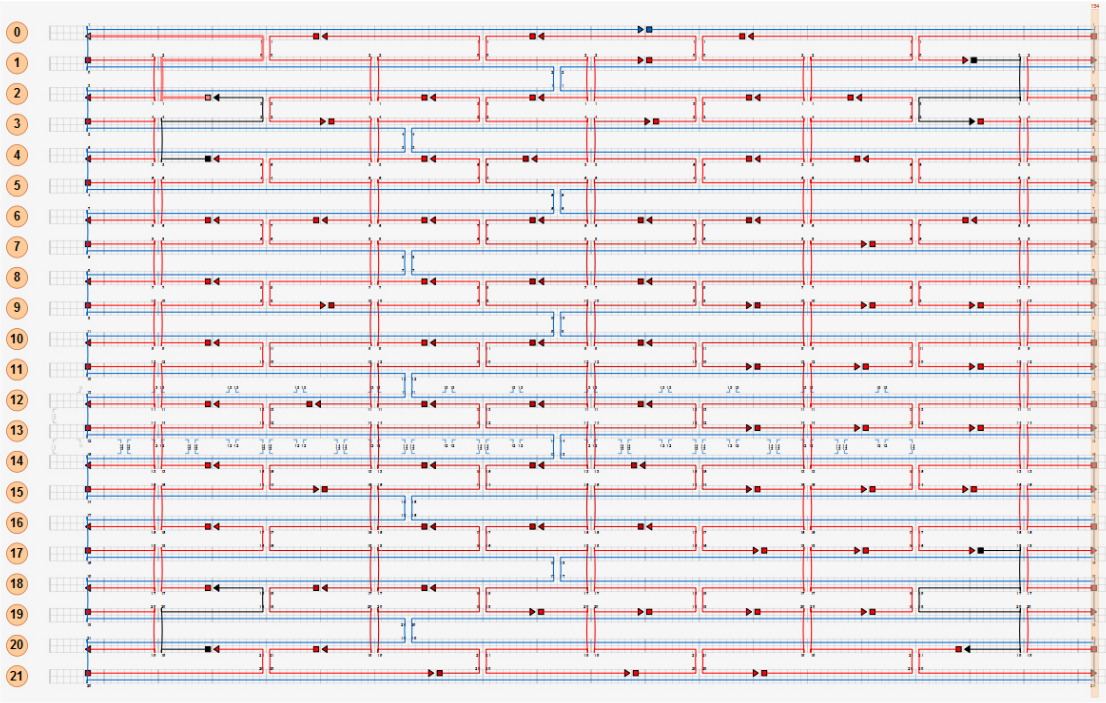

Figure S1. 2D map of the DNA origami nanoplate. The scaffold strand is shown in blue, and staple strands are in red. 5' and 3' termini of the DNA strands are represented as a squares and triangles, respectively. The numbering of duplexes is annotated at the left. The four black lines represent adapter staple oligonucleotides that carry a 3' overhang that can hybridize to the Alexa532-modified DNA oligonucleotide.

Table S1: Sequences of DNA Staple Strands

5' staple duplex number	3' staple duplex number	Sequence of oligonucleotides from 5' to 3' terminus
12[71]	14[72]	AGGAAGATCTGCTCATTCATAAATGCTGAGTG
0[71]	2[72]	ACAAACTAAACAGTTTCAGGTTTGATCCTCGG
15[121]	13[119]	CTCATATAGGCCGGAGACAGTCATCTACAAA
10[154]	9[154]	CGTCTGGCCTTAGTTTGAGGGG
2[55]	0[40]	AACAACTATTGCTAAACAACTTTCCAACGCCTGTAGCATTCCACAGAC
21[86]	19[87]	AAAAATCAGGAAGCAAACTCCAACAGGGATGGCT
1[5]	2[5]	TCGTCTTTCCAAAAATCTCCAA
6[39]	9[40]	ACAGCATCAGGAAGTTTCCATTAATACGTAATGCCACTACTTGACCCCC
15[136]	17[136]	TGCAATGCATCCAATAAATCATACAAGGTGGCA
19[104]	21[104]	AATATAATAAGCGAACCAGACCGGTCTTTACCC
3[89]	1[87]	GGGAGAGGCCCCAGCAGGCGAAAATGGTGGT
6[154]	5[154]	TTTTCCCAGTCCACACAACATA
9[121]	7[120]	CGCATCGTCGCACTCCAGCCAGCAGGGGGATG
21[5]	20[24]	TACTGCGGAATCGTCATAAATATTCATAAAATGTT
2[154]	1[154]	CTGATTGCCCTTGTTGTTCCAG
4[119]	2[119]	CTAATGAGGCGCCAGGGTGGTTTTAGAGAGTTG
10[55]	8[56]	GATAAATTATACCAAGCGCGAAACCATTCAGG

16[55]	14[56]	ACATTATAGCTCATTATGACCCTGTTGCCCTG
17[120]	15[120]	GAGCTGAAAGGCAAGGCAAAGAATTTTAGAACC
20[154]	19[154]	AAGCCCGAAAGAAAGTACGGTG
12[154]	11[154]	CAAGAGAATCGAAAATAATTCG
9[137]	11[136]	ATCTGCCCCTGTAGCCAGCTTTCAATAGGAAC
20[39]	21[56]	GTAATAGTTGAATCCCCCTCAAATGCTTTAAAC
16[23]	14[24]	ATCTACGTTTGTGAATTACCTTATAAATTGGG
7[5]	8[5]	GCTTTGAGGACAACGAAAGAGG
3[5]	4[5]	AAAAAAGGCTCAGTTGCGCCGA
19[88]	16[88]	TAGAGCTTTTTGACCATTAGATACTGGTCAATAACCTGTTTAAAGCCT
6[55]	4[56]	CCCTCAGCCGCTGAGGCTTGCAGGCGGGAAAC
8[55]	6[56]	CTGTAAAAACGGGCGCAACTGTTGGATCGTCA
18[39]	20[40]	ATAGTAAGAGAGGCTTTTGCAAAACAGAGGGG
0[102]	2[104]	AAAAACCCGGCAAAATCCCTTATCGGTCCAC
2[71]	4[71]	AGTGAGAAGCATTAATGAATCGGCCTGCCCGCT
13[120]	11[119]	GGCTATCAAAACTAGCATGTCAATAGCTCATT
14[154]	13[154]	GTAGGTAAAGATCTGGAGCAAA
11[137]	13[136]	GCCATCAATGAACGGTAATCGTAGGTCATTGC
4[55]	2[56]	CTGCTTTCGCTTGTCGTGCCAGCTTAGAAAGG
12[23]	10[24]	CGCATAGGGTCAATCATAAGGGAACCTGCTCC
15[5]	16[5]	AACTTTAATCATAATAAAACGA
9[41]	12[39]	AGCGATTGTGTCGAAATCCGCGACCGAACTGACCAACTTCAGATGAAC
19[72]	21[85]	ATTTTTGCGTCAGGATTAGAGAGTAAAACGAGAATGACCATAAATC
17[105]	19[103]	TTTCATTGAACGAGTAGATTTAGAATTGCTG
2[103]	4[104]	GCTGGTTTGCGGTTTGCGTATTGGTGAGCTAA
21[105]	19[120]	TGACTATTATAGTCAGAAGCAAATTTAATTCGAGCTTCAGCTGTAGCT
2[23]	0[5]	TCACGTTGGACGTTAGTAAATGAATAGTTAGCGTAACGATCTAAAGTTTTG
6[87]	3[88]	GAGGATCCAGCTCGAATTCGTAATAATTGCGTTGCGCTCACAACGCGCG
4[70]	6[72]	TTCCAGTGAGTTAAAGGCTACCGCCGGGCGC
17[5]	18[5]	ACTAACGGAACCCCTCGTTTAC
14[71]	16[72]	AATAAGGCTAATACTTTTGCGGGAAAAGCTAA
6[23]	4[24]	GGTAGCAAACCATCGCCCACGCATACAGCTTG
12[55]	10[56]	CAAGAGGATGAAAATATTTAAATTCATCGCCT
13[137]	15[135]	CTGAGAGTTCAAAAGGGTGAGAAATTTTAAA
7[121]	4[120]	TGCTGCAACGGCCAGTGCCAAGCTCCTGTGTGAAATTGTTGGGGTGC
21[57]	18[56]	AGTTCAGACCTTTAATTGTTTGCGAAGTCTCCTTTTGATTAACGCCA
0[154]	1[135]	TTTGGAACAAGAGTCCACTATTAAAGACCGAGATA
19[121]	17[119]	CAACATGTGATTCCCAATTCTGCTGGGGCGC
1[88]	0[72]	TCCGAAATGTCTATCAGAGTTTCGTCACCAGT
10[87]	8[88]	TCCGTGGGGGATTGACCGTAATGGTGGTGCCG
6[103]	9[103]	CTGCAGGTTACGCCAGCTGGCGAATTTCCGGCACCGCTTCGATAGGTC
4[154]	3[154]	CGAGCCGGAAGACGGGCAACAG
11[120]	9[120]	TTTTAACCATCAACATTAAATGTGGTAGATGGG
10[71]	12[72]	ATTTGTATGTAAACGTTAATATTTCCAAAAAC
18[154]	17[154]	TCTGGAAGTTTTACTAATAGTA
6[135]	9[136]	GTAAAACGAGGCGATTAAGTTGGGATCGGCCTCAGGAAGATAACCGTGC
3[137]	6[136]	CAGTGAGCATAAAGTGTAAAGCCTATCCGCTCACAATTCACGACGTT
13[5]	14[5]	TCATCAAGAGTGGTTTAATTTC
8[71]	10[72]	CCATTCGCAAAGTACAACGACGGCAACAAGAG
19[5]	20[5]	CAGACGACGATATAGCGTCCAA
5[5]	6[5]	CAATGACAACACGGCTACAGAG
12[87]	10[88]	GAAAAGCCTGTTAAAATTCGCATTTCGGATTC

3[41]	6[40]	TTTATCAGAGGTGAATTTCTTAAAACCGATATATTCGGTAGCGAAAG
2[118]	0[103]	CAGCAAGAAATCAAAAGAATAGCACGTGGACTCCAACGTCAAAGGGCG
6[71]	8[72]	TTTTGCGGGGAAGGGCGATCGGTGGCAAAGCG
0[39]	3[40]	AGCCCTCATTTTCTGTATGGGATTAAGGAATTGCGAATAATTGTATCGG
16[71]	19[71]	ATCGGTTGACATTCAACTAGCAAAATTTCATGCAGATACAAAGAGGTC
18[23]	16[24]	TATCATAAAACATTATTACAGGTAGAAGAAAA
12[38]	15[39]	GGTGTACGGATATTCATTACCCACACCAGAACGAGTAGTGCGATTTT
20[134]	21[154]	ATCGCGTGCGGATTGCATCAAAAAGATTAAGAGG
11[5]	12[5]	AGGCGCAGACGCTGGCTGACCT
9[104]	11[103]	ACGTTGGTAGCGAGTAACAACCCGAAATTTTT
16[87]	14[87]	CAGAGCATGAAGCCTTTATTTCAAATATTCAAC
14[55]	12[56]	ACGAGAAAAATCAACGTAACAAAGTGTATAAG
8[23]	6[24]	CAACCTAATAAAGACTTTTTCATGGGAACGAG
14[23]	12[24]	CTTGAGATAATCTTGACAAGAACCAGACCAGG
15[40]	18[40]	AAGAACTGCCAGTCAGGACGTTGGGAAAGATTCATCAGTTTACGAGGC
13[104]	15[103]	TTGAGAGAAATCACCATCAATATGCGCAAGGA
16[154]	15[154]	GTAGCATTAACCTGAGTAATGT
8[154]	7[154]	ACGACGACAGTTAACGCCAGGG
11[104]	13[103]	GTTAAATCCATATGTACCCCGGTTAGCTATTT
9[5]	10[5]	CAAAAGAATACTAGCCGGAACG
15[104]	17[104]	TAAAAATTTAGCAAAATTAAGCAATAGCTATAT
14[86]	12[88]	CGTTCTATAATGCCGGAGAGGGTGATAATCA
4[103]	6[104]	CTCACATTCATGGTCATAGCTGTTTTGCATGC
18[55]	16[56]	AAAGGAATGAGATTTAGGAATACCTACCAAAA
10[23]	8[24]	ATGTTACTACTAAAACACTCATCTGAAGGCAC
8[87]	6[88]	GAAACCAGCGGGCCTCTTCGCTATCGACTCTA

Table S2: Sequences of DNA Adapter Staple Strands

17[137]	20[135]	TCAATTCCATTCCATATAACAGTTTTTAAATATGCAACTACTTCAAAT TTTTGCCAAGATAGACAGAAGCGAG
4[23]	2[24]	ATACCGATCAAAAGGAGCCTTTAATAATTTTTTTTTGCCAAGATAGACAGAAGCGAG
20[23]	18[24]	TAGACTGGAAAAACCAAAATAGCGAGCAACACTTTTGCCAAGATAGACAGAAGCGAG
1[136]	3[136]	GGGTTGAGTCACCGCCTGGCCCTGTCTTTTCACTTTTGCCAAGATAGACAGAAGCGAG

1.3. PEG-Silanization of Substrates

ITO surfaces were cleaned to remove organic contaminants. The slides were incubated in 10 : 90, 50 : 50, and 90 : 10 methanol : $CHCl_3$ for 15 min each in an ultrasonic bath. After sonication, the slides were treated for 40 min at 70°C in basic Piranha (1:1:5 mixture of 30% ammonia and 30% hydrogen peroxide and water) that had been freshly prepared. After rinsing in deionized water and drying in a stream of nitrogen, the slides were plasma-oxidized in a Plasma System NANO (Diener electronic GmbH + Co. KG, Ebhausen, Germany) at 0.4 mbar for 2 minutes at 50 W. A layer of PEG-silane was grafted onto the ITO surface by immersing the slides in 20 mM PEG-silane in anhydrous toluene containing 5 % triethylamine as catalyst. The slides were incubated for 18 h at 60 °C, afterwards sonicated in toluene and ethanol for 5 min each to remove loosely bound PEG, and then rinsed with deionized water and dried in a stream of nitrogen. Silicon substrates were PEGylated following a similar procedure. Surfaces were first cleaned using ultra-sonication in acetone and then methanol for 15 min each, followed by incubation in basic Piranha (1:1:5 mixture of 30% ammonia and 30% hydrogen peroxide and water, freshly prepared) for 40 min at 70°C, and plasma-oxidation at 0.4 mbar for 5 min at 200 W. PEG was then grafted on the surface by overnight incubation in a 20 mM solution of PEG-silane in toluene supplemented with 0.08 % conc. HCl as catalyst, followed by washing as described above.

1.4. Electron-Beam-Induced Deposition (EBID)

EBID features were written with an e-beam lithography system eLINE Plus (Raith GmbH, Dortmund, Germany). The eLINE Plus is equipped with a GEMINI field-emitter column that allows for an electron beam size of 1.6 nm for electron energies > 3 keV. The background pressure during lithography was below 2 x 10^{-5} Torr in the sample chamber, and below 10^{-9} Torr at the cathode. The working distance during e-beam writing was chosen to be 10 mm. For a given beam current, typically around 0.0035 nA, doses per EBID feature were adjusted via the integral dwell time of the beam in each target area. Each series of arrays with systematically varying doses was written in one lithography run. The voltage used was 20 kV, the aperture 10 µm, measured current I=0.0035 nA, area dose 300 µC/cm^2, dot dose 0.029 pC. The e-beam lithography setup was operated in a Class 100 clean room.

1.5. Atomic Force Microscopy

For AFM analysis of DNA nanoplates, the origami structures were adsorbed onto mica following a modified version of a published procedure[1]. The purified plates were deposited onto freshly cleaned mica for 5 min, and images in liquid. All AFM topographical images of DNA origami were acquired *in situ* at RT using a Multimode AFM with a Nanoscope IV controller (Bruker Santa Barbara, US) and a reflective gold-coated (back side) MSNL E cantilever. The nominal spring constant of the MSNL cantilever was 0.06 N/m, and the resonance frequency was 7.3 kHz. Images were analyzed using Nanoscope Analysis software.

All AFM images of EBID nanopatterns were obtained with a Veeco Dimension 3100 (Bruker). As AFM probe, a rectangular cantilever AC160TS from Olympus micro cantilever (Shinjuku, Tokyo, Japan) with a tetrahedral tip for AC mode AFM measurements was used. The nominal spring constant of the silicon cantilever was 26 N/m, and the nominal length, width and thickness was 160 µm, 40 µm, and 370 nm, respectively. The tip length was 14 µm and the tip radius 7 nm.

1.6. Biofunctionalization of Nanoisland Arrays

To determine the influence of electron dose on protein adsorption (Figure 3), arrays of 100 x 100 nm-large nanoislands were incubated with 2 µM avidin-Cy3 in 0.1 x PBS buffer for 30 min. Subsequently, the surfaces were washed with 0.1 x PBS buffer (5 x 40 µL) and

deionized water (5 x 40 µL), dried in a stream of nitrogen, and immediately analyzed with fluorescence microscopy.

To generate nanoislands decorated with avidin and DNA origami (Figure 5), 100 x 100 nm islands were incubated with a 2 µM avidin solution in 0.1 x PBS buffer following the protocol described above. In a second step, the avidin-coated islands were incubated for 30 min with 7 nM fluorophore-tagged DNA nanoplates in TAE buffer (Tris base, acetic acid and EDTA, pH 8.0) supplemented with 14 mM $MgCl_2$. The samples were then washed and dried as described above.

To obtain nanoislands decorated with fluorescence-labeled streptavidin and optionally DNA origami nanoplates (Figure 6), island arrays were incubated with 2 µM avidin solution in 0.1 x PBS as described above. Half of the nanoislands were incubated with 7 nM DNA origami nanoplates in TAE buffer supplemented with 14 mM $MgCl_2$ following the protocol described above. In a last step, the decorated nanoislands were incubated for 30 min with fluorescence-labeled streptavidin in PBS buffer supplemented with 100 mM NaCl, followed by washing and drying.

1.7. Fluorescence Microscopy

Fluorescence images were obtained with an in-house developed fluorescence scanning device which is based on an inverted epifluorescence microscope (Axiovert 200, Zeiss, Oberkochen, Germany). For all measurements, a 100x objective (Zeiss, α Plan- FLUAR 100x/1.45) was used. Samples were mounted on a scanning stage (Märzhäuser, Wetzlar-Steindorf, Germany) and illuminated either with a diode-pumped solid-state laser with an emission line of 532 nm (Millennia Iis, Spectra Physics, Irvine, CA) or with a compact diode laser with an emission line of 646 nm (iBeam smart, Toptica photonics, Gräfeling, Germany). Images were taken with a Photometrics CoolSnap HQ digital camera (Roper Scientific, Trenton, NJ) (1392 x 1040-element CCD; pixel pitch, 6.45 mm x 6.45 mm; 12-bit; QE, 0.6) using a time delayed integration mode. Image processing and analysis were performed with ImageJ (NIH, Beteshda, USA) and Excel (Microsoft, Redmond, USA). In the quantitative analysis of fluorescence scans, affinity *A* was calculated from the difference of the average fluorescence of a 10 x 10 array of 100 x 100 nm^2 islands covering a total area of 39 x 39 μm^2, and the average background fluorescence from an proximal area without islands. Affinity thus represents the fluorescence of the island minus background. Sensitivity *S* was calculated from the ratio of the net fluorescence (affinity) over the background fluorescence, and normalized to the different areas of nanoislands vs. surrounding PEG-coated area. Contrast is obtained from the fluorescence peak profiles and defined as the net average difference between peak maxima and fluorescence background between peaks in the line profiles, divided by the net average difference between peak maxima and fluorescence background outside the line profiles.

2. Experimental Results

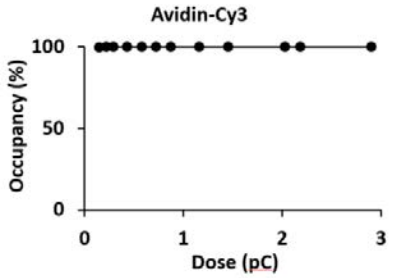

Figure S2. Mean occupancy of avidin-Cy3 for 100 x 100 nm EBID nanoisland arrays as a function of EBID electron dose. Occupancy is defined as the percentage of nanoislands in a 10 x 10 array that are decorated with fluorophore-labeled protein. An island is considered to be decorated with avidin-Cy3 when the fluorescence intensity of the island is higher than the fluorescence background plus three times the standard deviation of the background fluorescence. The data represent the means and standard deviations obtained from eight independent experiments.

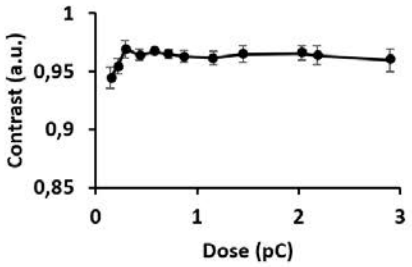

Figure S3. Mean contrast factor for avidin-Cy3 coated 100 x100 nm EBID nanoislands as a function of electron dose (n = 8). Contrast is defined in SI section 1.7.

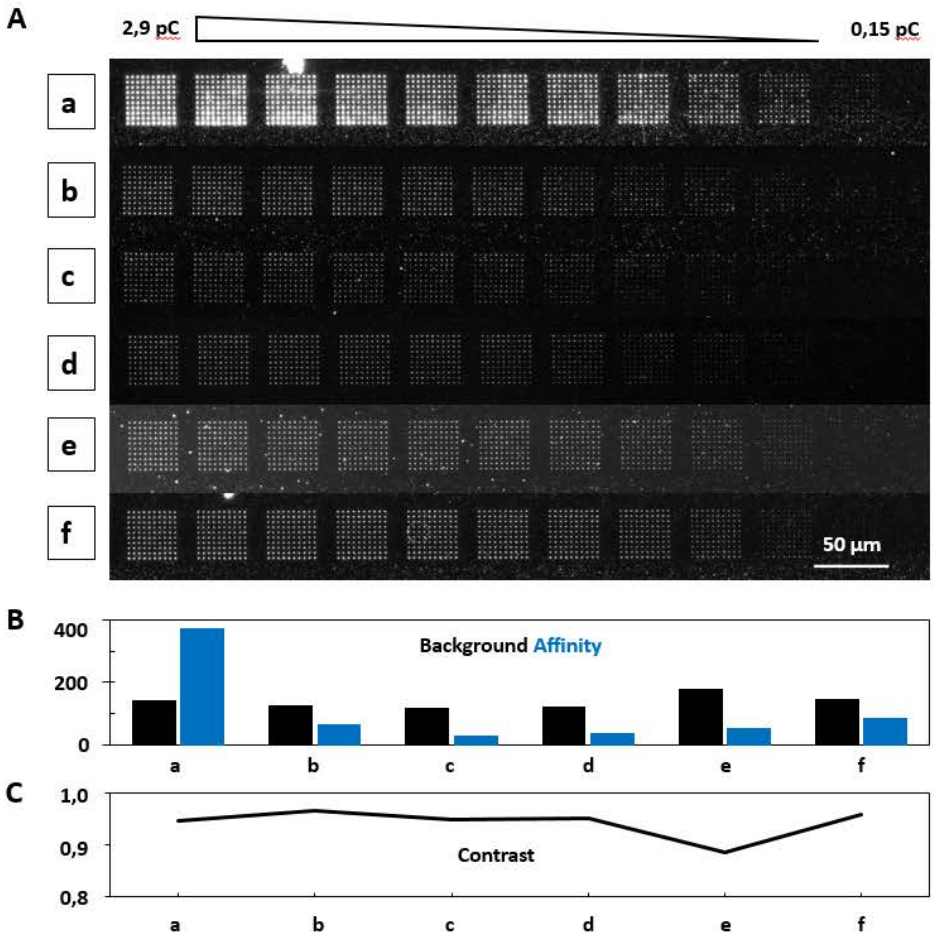

Figure S4. The binding of avidin-Cy3 to EBID nanoarrays is influenced by different buffer conditions including buffer components, ionic strength and pH. (A) Fluorescence micrographs of nanoarrays of 10 x 10 islands of 100 x 100 nm size written at an electron dose ranging from 2.9 to 0.15 pC. The incubation conditions were (a) 0.1 x PBS, (b) PBS, (c) PBS + 100 mM NaCl, (d) TE + 100 mM NaCl pH 8.0, (e) TE + 100 mM NaCl pH 10, and (f) TE pH 8.0. Condition (a) (0.1 x PBS) was used for experiments shown in the main manuscript. (B, C) The background (B) and affinity (C) depends on the different incubation conditions (a-e). Background is defined as the average fluorescence counts of areas next to islands. Affinity and contrast are defined in section 1.7 of the SI.

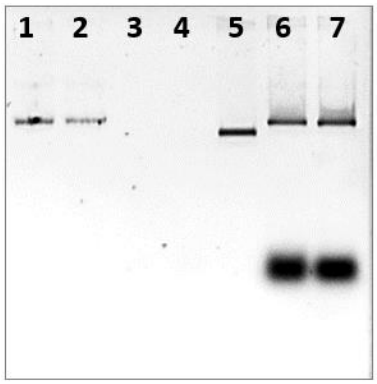

Figure S5. Analysis of DNA origami nanoplates after purification with filter units with a molecular weight cut-off at 100 kD. Lanes 1&2, purified DNA origami plates; lanes 3&4, flow-through containing excess staples; lanes 5, scaffold m13mp18; lanes 6&7, DNA origami plates and excess staple strands prior to purification.

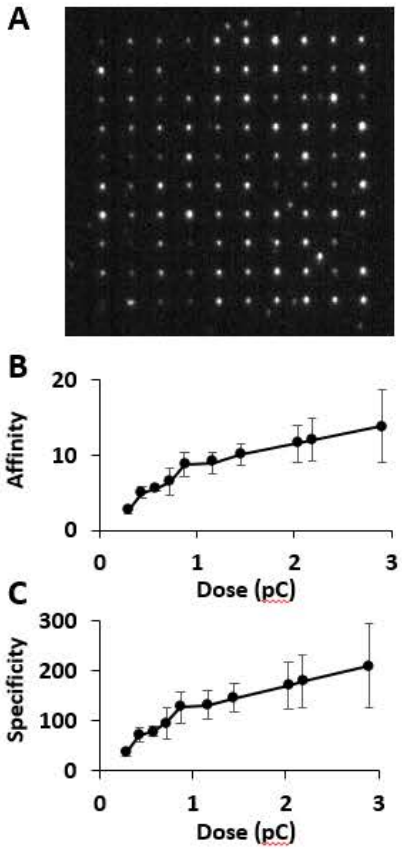

Figure S6. A fluorophore-labeled 18-mer DNA oliognucleotide binds electrostatically avidin-coated carbon nanoislands. The 18-mer with the sequence 5'-CAC TGG CAA CAT TGC GGA-3' carries at its 5'-terminus a Cy5 dye via TEG linker. (A) Fluorescence microscopic image of an array of 100 x 100 nm islands written at a dose of 2.9 pC (image size: 39 x 39 µm). No binding occurs when the nanoislands are bare and not coated with avidin (data not shown). (B) Affinity and (C) specificity for the binding of fluorescent labeled DNA to the nanoislands. Affinity and specificity are defined in section 1.7 of the SI. The data represent the means and standard deviations obtained from three independent experiments.

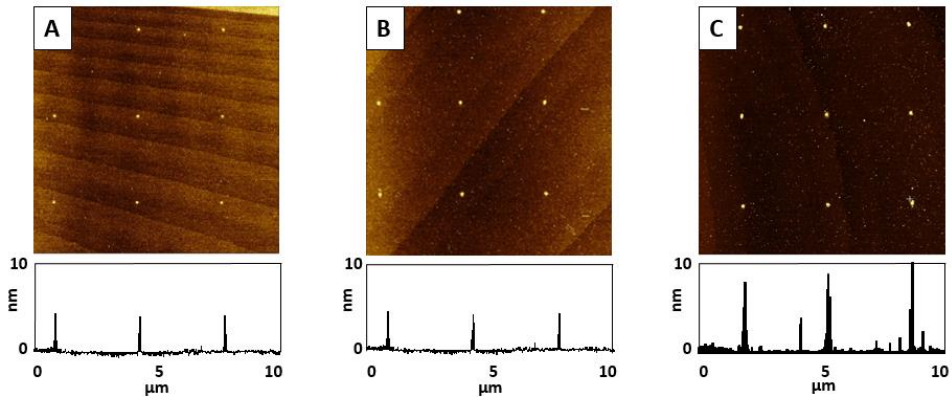

Figure S7. AFM analysis of a 3 x 3 array of 50 nm EBID nanoislands written at a dose of 1.16 pC, with optional incubation with avidin and DNA origami nanoplates. (A) Nanoarray prior to incubation, displaying an island height of 3.3 ± 0.5 nm. (B) Incubation with avidin increases the total island height of 4.4 ± 1.5 nm. (C) Incubation with avidin proteins and DNA origami plates yields a height of 8.2 ± 3.6 nm. The binding of protein (4 x 5 x 6 nm) leads to a smaller than expected average height increase but is within error. Similarly, the binding of DNA origami (2 nm height) is associated with a larger height increase but within error. The data could also indicate that the DNA nanoplates may deviate from the flat rectangular shape and are more corrugated.

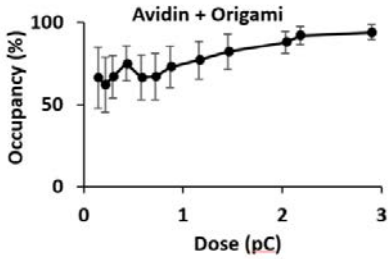

Figure S8. The occupancy of avidin-coated nanoislands for fluorophore-labeled DNA nanoplates depends on electron dose for writing 100 x 100 nm EBID nanostructures. Occupancy is defined as the percentage of nanoislands in a 10 x 10 array that are decorated with fluorophore-labeled DNA origami. An island is considered to be decorated with DNA origami when the fluorescence intensity of the island is higher than the fluorescence background plus three times the standard deviation of the background fluorescence. The data represents the means and standard deviations obtained from eight independent experiments.